Geomechanics and Engineering, *Vol. 25, No. 6 (2021) 509-520*
DOI: https://doi.org/10.12989/gae.2021.25.6.509

Shapes and formation mechanism of the plastic zone surrounding circular roadway under partial confining stress in deep mining

Xiaofei Guo*, Chen Li and Tianhong Huo

School of Energy & Mining Engineering, China University of Mining and Technology (Beijing), Beijing 100083, China

(Received October 7, 2020, Revised May 24, 2021, Accepted June 14, 2021)

Abstract. To reveal the failure mechanism of roadway surrounding rock under the partial confining stress in deep mining, by means of theoretical analysis and numerical simulation, this paper studied the distribution laws of the principal stress field around the circular hole and compared the shapes of the plastic zone surrounding rock under the same conditions. The results show that: under hydrostatic stress (λ=1), the circumferential principal stress around the hole is the same everywhere, and the shape of plastic zone is circular; under low partial confining stress ($1<\lambda<2$), the rock element at the abscissa axis is most likely to be destroyed, while it is the least likely to be destroyed at the ordinate axis, resulting in the formation of an elliptical plastic zone; under high partial confining stress ($\lambda\geq2$), the rock elements near the middle axis are easier to be destroyed, while the destructive force decreases gradually when it approaches the two axes, resulting in the formation of a butterfly plastic zone. The lateral stress coefficient is the main factor causing the butterfly failure of the roadway surrounding rock. And the depth is the main factor causing the large-scale failure of the roadway surrounding rock. Under the condition of deep and high partial confining stress, the roadway surrounding rock will appear large-scale and butterfly failure zone.

Keywords: partial confining stress; plastic zone shape; lateral stress coefficient; circular roadway; deep mining

1. Introduction

The large deformation, roof fall and dynamic disaster in roadway are the major problems that perplex and restrict the safe and efficient mining (Yang *et al.* 2017a, Yang *et al.* 2017b, Diederichs 2018). With the continuous increase of mining depth, a series of surrounding rock instability problems become more and more prominent (Konicek *et al.* 2013, Lamich *et al.* 2016, Feng *et al.* 2018). According to the mechanism analysis of disaster mechanics, the large deformation, roof fall and rock burst in roadway are caused by the destruction of surrounding rock in different ranges and forms (Palumbo *et al.* 2017, Paul 2016, Vazaios *et al.* 2019). The shape characteristics and evolution law of failure zone have a direct impact on the type and severity of disasters (Leitman and Villaggio 2009, Li *et al.* 2020).

For a long time, Kastner formula or Fenner formula has been used to calculate the plastic zone of the roadway surrounding rock theoretically (Kastner 1971, Fan *et al.* 2013). These formulas are based on the uniform stress environment, and the calculated plastic zone shape is circular. However, the stress environment of most underground engineering is non-uniform (Detournay and John 1988, Fan and Liu 2019, Atsushi *et al.* 2020, Vitali *et al.* 2020). Especially, affected by mining activities, the local mined out area will cause stress relief in one direction and stress concentration in another direction (Liu *et al.* 2012). As a result, the stress in different directions varies greatly, and the partial confining stress environment will be formed (Kang *et al.* 2010, Garavand *et al.* 2020, Li *et al.* 2019). Therefore, we define the stress field with different stresses in different directions around the roadway as partial confining stress. Similarly, in the vicinity of the geological structure belt, due to the stress compression in one direction, the stress deviation in different directions is large, and the stress shows the characteristics of non-uniform distribution (Vidigal-Souza *et al.* 2020). There will be plastic zones with different shapes in the surrounding rock of roadway in non-uniform stress field (Ding and Liu *et al.* 2018). The literatures (Aker *et al.* 2014, Zhu *et al.* 2020) studied the acoustic emission test of sandstone samples with a circular hole and found that the surrounding rock would appear X-type failure under uniaxial compression. The literature (Wang *et al.* 2020) found that the failure mode of surrounding rock under biaxial unequal stress presents a non-uniform shape. Others (Ma *et al.* 2015, Guo *et al.* 2016) found that there were circular, elliptical and butterfly shaped plastic zone in the roadway surrounding rock in the non-uniform stress field. These research results are obtained through laboratory test or numerical simulation. The different failure modes and plastic zone shapes obtained are only visual fuzzy discrimination. The mechanical behavior of different shapes plastic zone in non-uniform stress field is still unclear, and the strict mechanical definition of different shapes plastic zone is also not clear.

Affected by mining or located near the geological structure area, the roadway often deforms seriously and is prone to roadway disasters (Rezaei *et al.* 2015). In the deep condition, the stress level will increase, and the roadway will inevitably be affected by mining and in partial confining stress conditions (Tian *et al.* 2020). The research

*Corresponding author, Ph.D.
E-mail: 15201290185@163.com

ISSN: 2005-307X (Print), 2092-6219 (Online)

on the failure mechanism of roadway surrounding rock under high stress and partial confining stress will help to reveal the mechanism of roadway disaster under deep mining conditions.

To reveal the failure mechanism of roadway surrounding rock under the partial confining stress in deep mining, according to the plane strain model, this paper studied the shapes evolution of the plastic zone surrounding the circular roadway with the variation of the lateral stress coefficient. In addition, the formation mechanism of different plastic zone shapes was revealed on the basis of the distribution laws of the principal stress field around the circular hole under the condition of partial confining stress.

2. Methods

2.1 Theoretical model

The roadway is located in the complex underground stress and surrounding rock environment. Under the existing mathematical and mechanical conditions, the plane strain model with circular hole is usually used to study the elastic-plastic problem of underground roadway surrounding rock (Hill 1950). In the infinite underground space environment, the roadway can be regarded as a long hole with uniform distribution. So we can take any section of roadway as its representative to study. Due to the influence of structure and mining, the in-situ stress presents the characteristics of non-uniform distribution and the stress in different directions is often different (Kang *et al.* 2010, Li *et al.* 2019). Therefore, we established the plane strain force model of roadway surrounding rock in non-uniform stress field, as shown in Fig. 1.

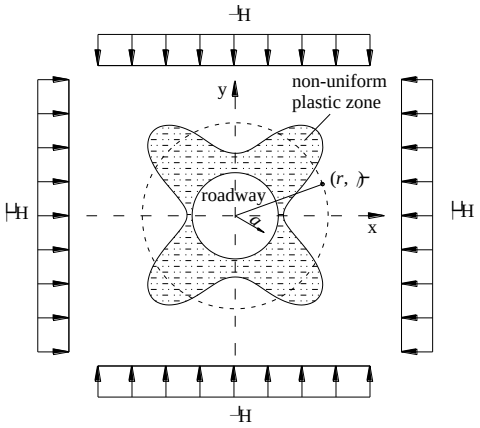

Fig. 1 Force model of roadway in partial confining stress field

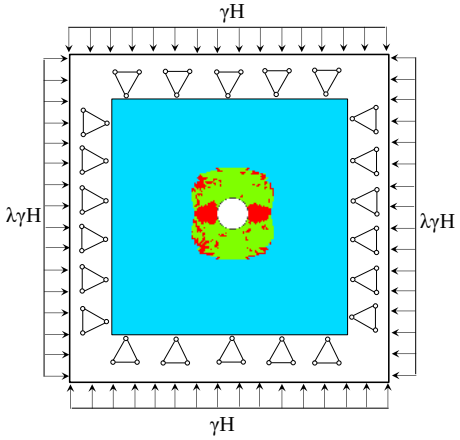

Fig. 2 Plane numerical simulation force model

In the figure, H is the depth of the roadway, m; γ is the rock bulk density, KPa/m; and the product of the two is the stress of the model in the vertical direction; λ is the lateral stress coefficient, and its product with the vertical stress is the horizontal stress of the model, so the lateral stress coefficient represents the difference level of stress in two directions; r and θ are the polar coordinates, m and rad; a is the roadway radius, m. In this model, the depth of roadway is considered, and the non-uniform distribution characteristics of in-situ stress are also fully considered.

According to the plane strain model with circular hole and the Mohr-Coulomb strength theory, the boundary equation of the plastic zone surrounding the circular roadway in non-uniform stress field was deduced (Poulos and Davis 1974). We can study the shape of plastic zone on the basis of the boundary equation. The expression is as follows:

$$
\begin{aligned}
&9(1-\lambda)^2\left(\frac{a}{r}\right)^8+\left[-12(1-\lambda)^2+6(1-\lambda)\cos 2\theta\right]\left(\frac{a}{r}\right)^6\\
&+\left[\begin{matrix}10(1-\lambda)^2\cos^2 2\theta-4(1-\lambda)^2\sin^2\varphi\cos^2 2\theta\\-2(1-\lambda)^2\sin^2 2\theta-4(1-\lambda^2)\cos 2\theta+(1+\lambda)^2\end{matrix}\right]\left(\frac{a}{r}\right)^4\\
&+\left[\begin{matrix}-4(1-\lambda)^2\cos 4\theta+2(1-\lambda^2)\cos 2\theta\\-4(1-\lambda^2)\sin^2\varphi\cos 2\theta-\dfrac{4C(\lambda-1)\sin 2\varphi\cos 2\theta}{\gamma H}\end{matrix}\right]\left(\frac{a}{r}\right)^2\\
&+\left[(1-\lambda)^2-\sin^2\varphi\left(1+\lambda+\frac{2C\cos\varphi}{\gamma H\sin\varphi}\right)^2\right]=0
\end{aligned}
\tag{1}
$$

where φ is the rock internal friction angle, rad; C is the rock cohesion, MPa.

2.2 Numerical simulation model

In order to make the results reliable, the method of combining theoretical analysis and numerical simulation was used to analyze the plastic zone shape of the roadway surrounding rock in this study (Jiang *et al.* 2016). The FLAC^{3D} numerical simulation software was adopted, and the numerical simulation model is shown in Fig. 2.

Based on the existing numerical simulation results (Ma *et al.* 2015, Guo *et al.* 2016), when it is fixed by displacement in the axial direction of roadway, the boundary effect of model thickness on surrounding rock failure range is not obvious, and the shape and size of plastic zone with different thickness and cross-section are almost the same in the axial direction of roadway. Therefore, the numerical simulation model established in this paper adopts the thin plate stress model constrained by displacement in the axial direction of roadway. The side length of the model is more than 40 times of the hole diameter to ensure that the model size is large enough. Based on Saint-Venant's principle, the influence of roadway on the model boundary can be ignored in enough underground space, so the boundary around the model is

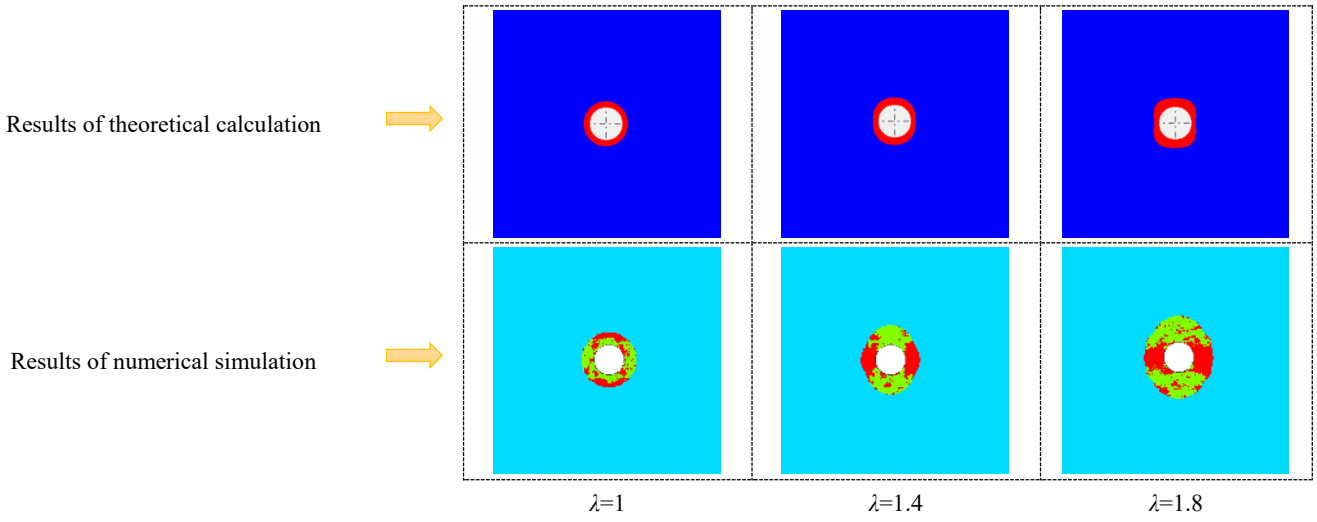

(a) Evolution of elliptical plastic zone

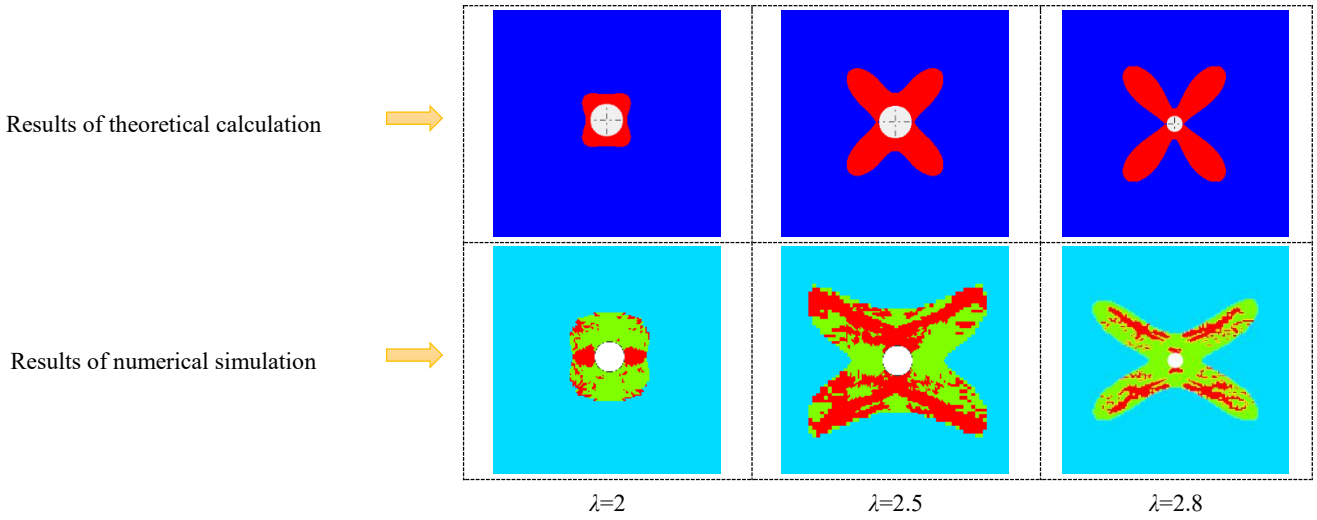

(b) Evolution of butterfly plastic zone

Fig. 3 Shapes evolution of the roadway plastic zone

constrained by displacement and loaded with the initial command (Maihemuti *et al.* 2016).

3. Shape evolution of the roadway plastic zone under partial confining stress

3.1 Shape evolution of the roadway plastic zone

Due to the influence of structure and mining, the in-situ stress presents the characteristics of non-uniform distribution and the stress in different directions is often different. The lateral stress coefficient is often not 1, and the stress in one direction is several times that in the other in the force model, so the partial confining stress state is formed. To obtain the shape evolution of the roadway plastic zone under partial confining stress, we study the effect of lateral stress coefficient on the shape of plastic zone on the basis of the plane strain model in Fig. 1-2. According to the present observation data of in-situ stress, the lateral stress coefficient increases gradually from 1 in this study; 800 m is taken as the reference level of the roadway depth, and the average value of 25 KPa/m is taken as the bulk density (Hill 1950); the roadway radius is 2 m, and The parameters of surrounding rock in the model are determined by referring to the parameters of coal (Guo *et al.* 2016), as shown in Table 1. The results are shown in Fig. 3.

Table 1 The parameters of surrounding rock

Internal friction angle /°	Cohesion /MPa	Density /(kg/m3)	Elastic modulus /GPa	Poisson's ratio	Uniaxial compressive strength / MPa
25	3.0	1400	22.96	0.23	9.42

From Fig. 3, we can see that with the increase of lateral stress coefficient from 1, there are three shapes of plastic zone and two evolution stages. The three shapes are circular, elliptical and butterfly, and the two evolution stages include ellipse evolution and butterfly evolution. At the same time, the results of theoretical calculation and

numerical simulation are in good agreement. (1) When the lateral stress coefficient is 1, the model is under hydrostatic stress, and the shape of plastic zone is circular; (2) with the lateral stress coefficient increasing from 1, the range of the plastic zone in the longitudinal direction gradually increases, while in the transverse direction it gradually decreases. The boundary of the plastic zone transits smoothly, and gradually evolves from a circle to an ellipse; (3) when the lateral stress coefficient exceeds 2, the maximum radius of the plastic zone gradually moves from the longitudinal axis to the middle of the quadrant, and the plastic zone is a butterfly shape with depression at the coordinate axis and protruding in four quadrants; (4) after the butterfly shaped plastic zone appears, the plastic zone expands in butterfly shape with the increase of lateral stress coefficient before the model failure.

3.2 Mechanical meaning of plastic zone with different shapes

With the increase of lateral stress coefficient from 1, the shape of plastic zone will be circular, elliptical and butterfly. However, these shapes are merely sensory visual descriptions, not strictly mechanical definitions. The results of theoretical calculation and numerical simulation are in good agreement in Fig. 3. So, each shape may have a strictly mechanical meaning. The boundary equation of plastic zone represents the set of all points satisfying the Mohr Coulomb criterion, so Formula (1) represents the relationship between r and θ on the boundary of plastic zone. The formula (1) is the 8 square function of r, at the same time, it can be transformed into an equation about θ, as shown in formula (2).

$$f(\cos 2\theta) = m_1 \cos^2 2\theta + m_2 \cos 2\theta + m_3 = 0 \tag{2}$$

where

$$m_1 = \left[12(1-\lambda)^2 - 4(1-\lambda)^2 \sin^2\varphi\right](\frac{a}{r})^4 - 8(1-\lambda)^2(\frac{a}{r})^2;$$

$$m_2 = 6(1-\lambda^2)(\frac{a}{r})^6 - 4(1-\lambda^2)(\frac{a}{r})^4 + \left[2(1-\lambda^2) - 4(1-\lambda^2)\sin^2\varphi - \frac{4C(\lambda_1-1)\sin 2\varphi}{\gamma H}\right](\frac{a}{r})^2;$$

$$m_3 = 9(1-\lambda)^2(\frac{a}{r})^8 - 12(1-\lambda)^2(\frac{a}{r})^6 + \left[(1+\lambda)^2 - 2(1-\lambda)^2\right](\frac{a}{r})^4 + 4(1-\lambda)^2(\frac{a}{r})^2 + (1-\lambda)^2 - \sin^2\varphi(1+\lambda+\frac{2C\cos\varphi}{\gamma H\sin\varphi})^2$$

When the lateral stress coefficient is 1, the formula (2) is a standard equation of circle about r. When the lateral stress coefficient is not 1, the formula (2) is a quadratic equation about $\cos 2\theta$. Giving any r in circular direction, when the formula (2) has only one real root about $\cos 2\theta$, there will be four θ corresponding to one r, and the shape of plastic zone is elliptical, as shown in the Fig. 4(b); when the formula (2) has two real roots about $\cos 2\theta$, there will be eight θ corresponding to one r, and the shape of plastic zone is butterfly, as shown in the Fig. 4(c). Therefore, the shape of plastic zone is elliptical and the boundary equation has only one real root about $\cos 2\theta$, while the shape of plastic zone is butterfly and the boundary equation has two real roots about $\cos 2\theta$.

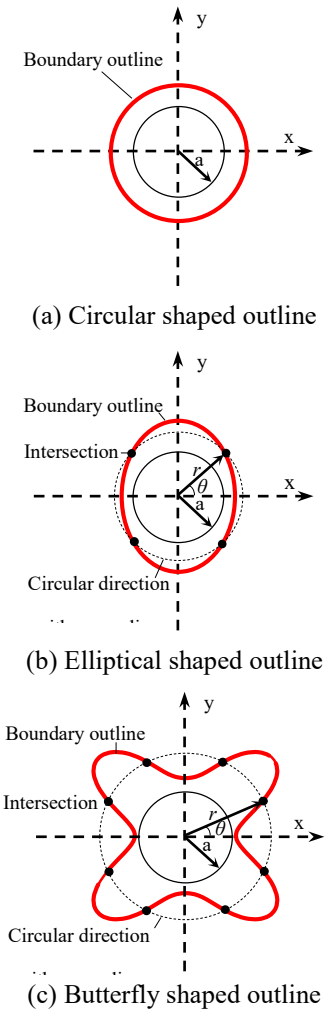

Fig. 4 Mechanical meaning diagrams of plastic zone with different shapes

4. Formation mechanism of plastic zones with different shapes

4.1 Rock strength criterion

In this study, the Mohr-Coulomb strength criterion is used to analyze the plastic zone of surrounding rock. According to the Mohr-Coulomb strength criterion, the failure state of rock element depends on the relative position between Mohr circle and rock envelope, as shown in Fig. 5. In the Figure, σ_1 is the maximum principal stress of the element, and σ_3 is the minimum principal stress of the element. When Mohr circle intersects or tangent to the envelope of rock, the rock element is in plastic state; when they are separated, the rock element is in elastic state. When the lithology of surrounding rock is determined, the character of Mohr circle determines the failure state of rock element. In other word, the larger the Mohr circle radius is

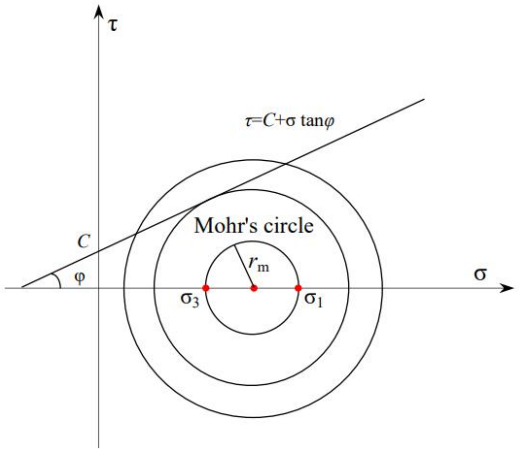

Fig. 5 Mohr-Coulomb strength criterion

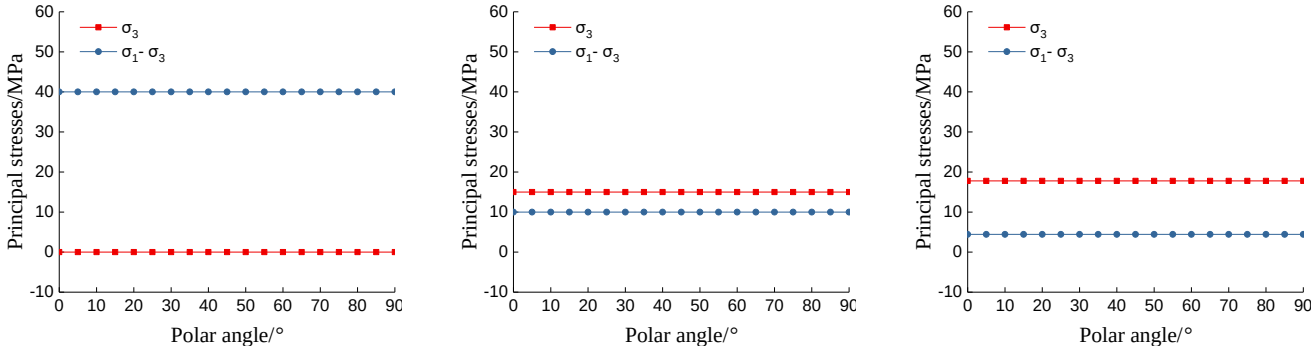

(a) r/a=1 (b) r/a=2 (c) r/a=3

Fig. 6 Distribution of principal stress field around a circular hole under hydrostatic stress (λ=1)

and the closer the circle center is to the origin, the more likely the rock element will be destroyed. We use r_m represent the Mohr circle radius, and it can be expressed as formula (3). The maximum principal stress and minimum principal stress determine the character of Mohr circle. In the following, we will study the distribution of principal stress around a circular hole under partial confining stress.

$$r_m = (\sigma_1 - \sigma_3)/2 \tag{3}$$

4.2 Distribution law of principal stress field in circular direction

According to the plane strain force model in non-uniform stress field in Fig. 1, combining with previous results of elastic mechanics (Poulos and Davis 1974), the stress solutions at any point around a circular hole were obtained, as expressed in formula (4).

$$\begin{cases} \sigma_r = \dfrac{\gamma H}{2}\left[(1+\lambda)\left(1-\dfrac{a^2}{r^2}\right)+(\lambda-1)\left(1-4\dfrac{a^2}{r^2}+3\dfrac{a^4}{r^4}\right)\cos 2\theta\right] \\ \sigma_\theta = \dfrac{\gamma H}{2}\left[(1+\lambda)\left(1+\dfrac{a^2}{r^2}\right)-(\lambda-1)\left(1+3\dfrac{a^4}{r^4}\right)\cos 2\theta\right] \\ \tau_{r\theta} = \dfrac{\gamma H}{2}\left[(1-\lambda)\left(1+2\dfrac{a^2}{r^2}-3\dfrac{a^4}{r^4}\right)\sin 2\theta\right] \end{cases} \tag{4}$$

where σ_r, σ_θ and $\tau_{r\theta}$ are the radial, tangential and shearing stresses, respectively, at any point with polar coordinates (r, θ) around the circular hole. According to the stress solutions around a circular hole, we can get the principal stress at any point, as expressed in formula (5).

$$\begin{cases} \sigma_1 = \dfrac{\sigma_r + \sigma_\theta}{2} + \dfrac{1}{2}\sqrt{(\sigma_r - \sigma_\theta)^2 + 4\tau^2_{r\theta}} \\ \sigma_3 = \dfrac{\sigma_r + \sigma_\theta}{2} - \dfrac{1}{2}\sqrt{(\sigma_r - \sigma_\theta)^2 + 4\tau^2_{r\theta}} \end{cases} \tag{5}$$

According to the formulas (4) and (5), we can see that the main factors affecting the principal stress around the hole are depth (H), lateral stress coefficient (λ) and location (r, θ). The maximum principal stress and minimum principal stress determine the character of Mohr circle on basis of the Mohr-Coulomb strength criterion, as shown in Fig. 5. The smaller the minimum principal stress is and the larger the Mohr circle radius is, the easier the rock element will be destroyed. Therefore, we will study the distribution of the principal stress field around the circular hole under partial confining stress to reveal the formation mechanism of the plastic zone with different shapes. Based on the symmetry of the stress model (shown in Fig. 1-2), we only study the stress distribution in the first quadrant ($0<\theta<90°$). According to shapes evolution of the plastic zone with lateral stress coefficient (shown in Fig. 3), we will explain the distribution of stress field in three cases: hydrostatic

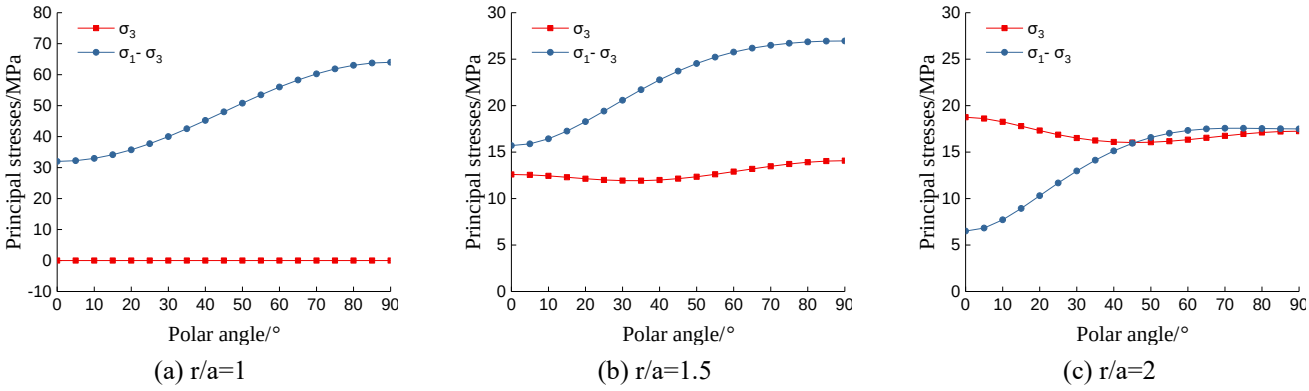

(a) r/a=1 (b) r/a=1.5 (c) r/a=2

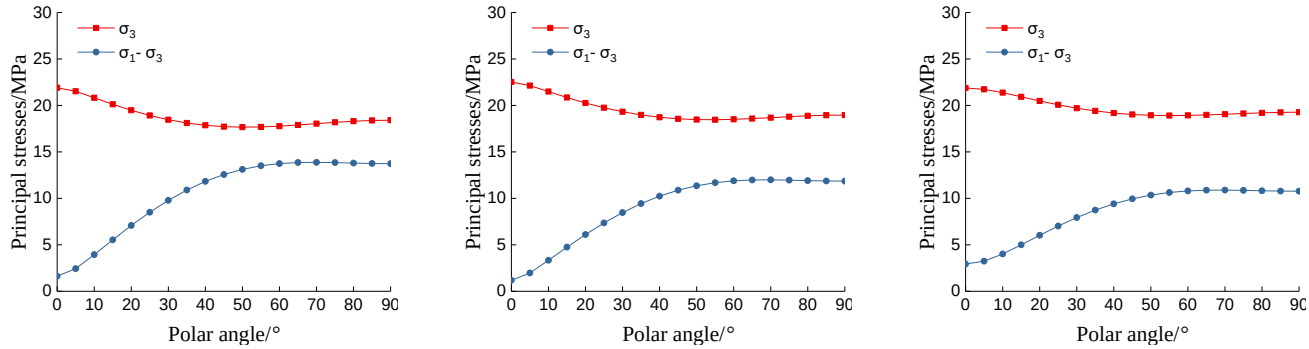

(d) r/a=2.5 (e) r/a=3 (f) r/a=3.5

Fig. 7 Distribution of principal stress field around a circular hole under low partial confining stress (λ=1.4)

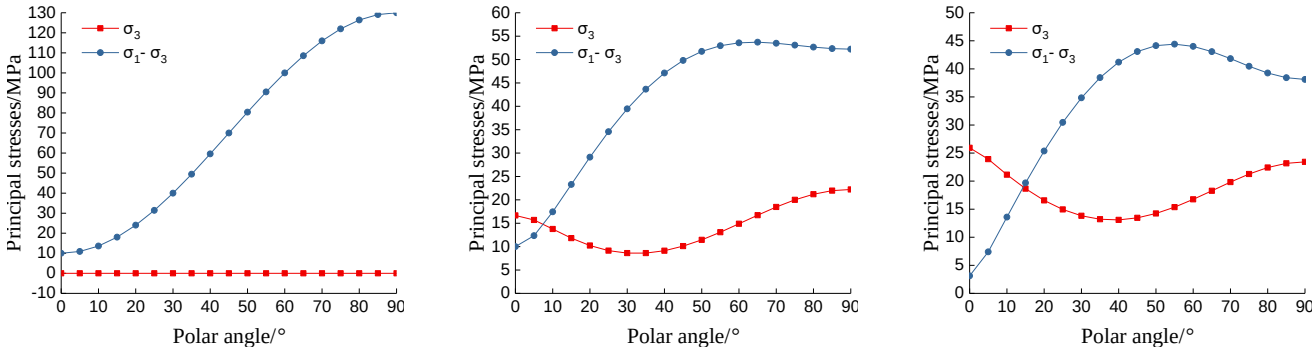

(a) r/a=1 (b) r/a=1.5 (c) r/a=2

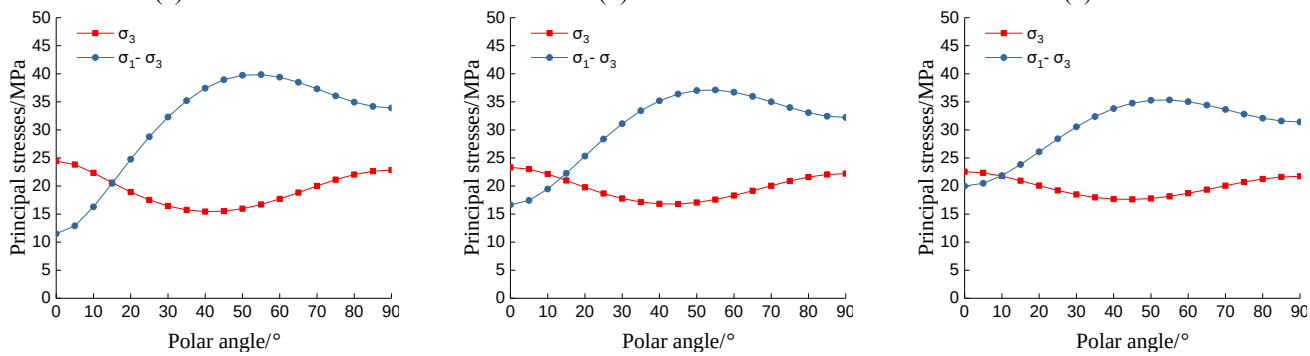

(d) r/a=2.5 (e) r/a=3 (f) r/a=3.5

Fig. 8 Distribution of principal stress field around a circular hole under high partial confining stress (λ=2.5)

stress state, low partial confining stress state and high partial confining stress state.

4.2.1 Hydrostatic stress state (λ=1)

Taking the depth of 800 m as an example, we study the variation of principal stress with polar angle in different radial directions in the first quadrant under hydrostatic stress, as shown in Fig. 6. We can see that the principal stresses do not change with the change of circumferential position when the radial position is determined. In other

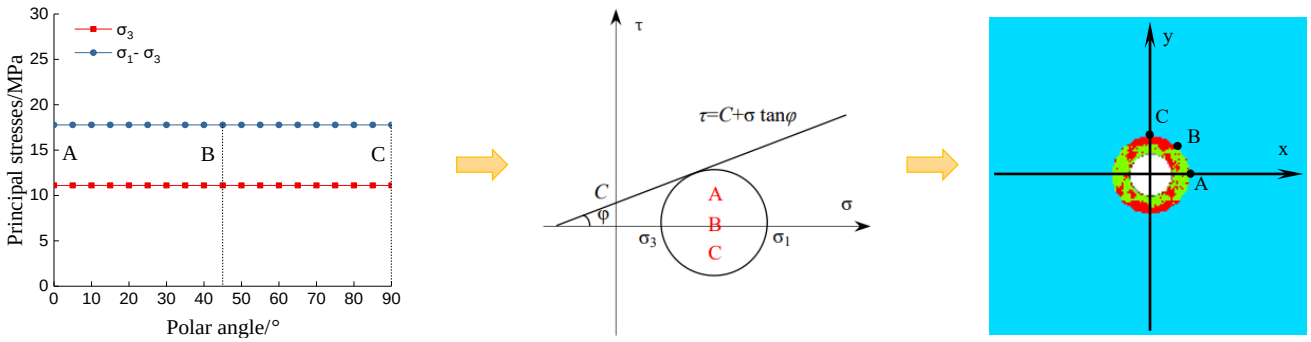

(a) Distribution of principal stress (b) Strength criterion (c) Circular plastic zone

Fig. 9 Formation mechanism of circular plastic zone

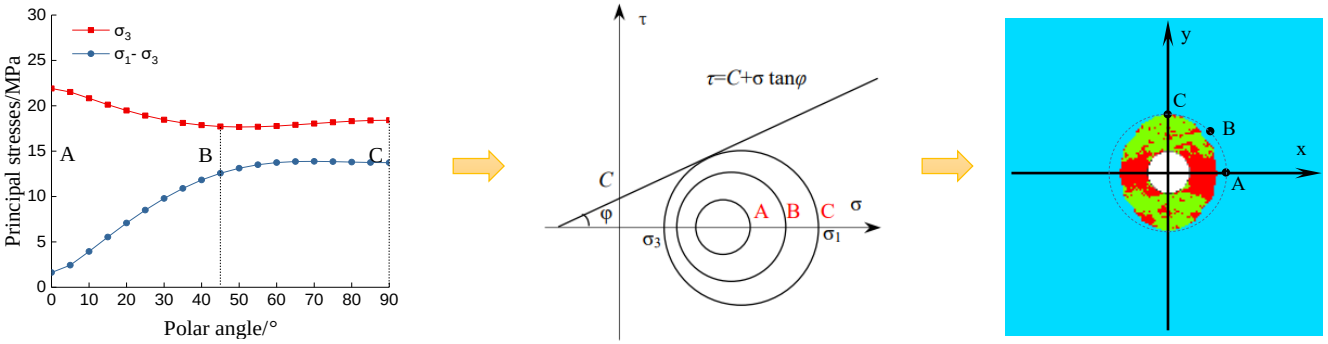

(a) Distribution of principal stress (b) Strength criterion (c) Circular plastic zone

Fig. 10 Formation mechanism of elliptical plastic zone

words, the circumferential principal stress around the hole is the same everywhere. In the radial direction, with the increase of the distance from the center of the circle, the minimum principal stress increases and the difference of the principal stress decreases.

4.2.2 Low partial confining stress state (1<λ<2)

According to shapes evolution of the plastic zone with the lateral stress coefficient as shown in Fig. 3, when the lateral stress coefficient is less than 2, the shape of plastic zone is elliptic; when the lateral stress coefficient is greater than 2, the shape of plastic zone is butterfly. So we define the stress state with the lateral stress coefficient less than 2 as low partial confining stress state, and stress state with the lateral stress coefficient greater than 2 as high partial confining stress state. Taking the depth of 800 m and the lateral stress coefficient of 2 as an example, we study the variation of principal stress with polar angle in different radial directions in the first quadrant under low partial confining stress, as shown in Fig. 7. We can see that the variation of principal stresses with polar angle is the same in different circumferential positions. In the circumferential direction, the minimum principal stress decreases with the polar angle, and the principal stress difference increases with the polar angle.

4.2.3 High partial confining stress state (λ>2)

Similarly, taking the depth of 800 m as an example, we study the variation of principal stress with polar angle in different radial directions in the first quadrant under high partial confining stress, as shown in Fig. 8. We can see that the variation of principal stresses with polar angle is the same in different circumferential positions when *r*/*a* is greater than 1. In the circumferential direction, the minimum principal stress decreases first and then increases with the polar angle, showing the characteristics of concave function; the principal stress difference increases first and then decreases with the polar angle, showing the characteristics of convex function. The distribution of principal stress field under high and low partial confining stress is obviously different.

4.3 Mechanical mechanism of plastic zone with different shapes

According to the distribution of the principal stress field around the hole under different confining stress and the Mohr-Coulomb strength criterion, we will explain the formation mechanism of plastic zone with different shapes in three cases.

4.3.1 Mechanical mechanism of circular plastic zone

The shape of plastic zone is circular when the model is under hydrostatic stress (λ=1). Based on the above research results, the circumferential principal stress around the hole is the same everywhere, as shown in Fig. 9(a). The Mohr's circle is exactly the same everywhere in the circumferential direction (A. B and C represent any three points in the circumferential direction), as shown in Fig. 9(b). The failure force of circumferential stress on rock is the same everywhere, and uniform failure occurs around the hole,

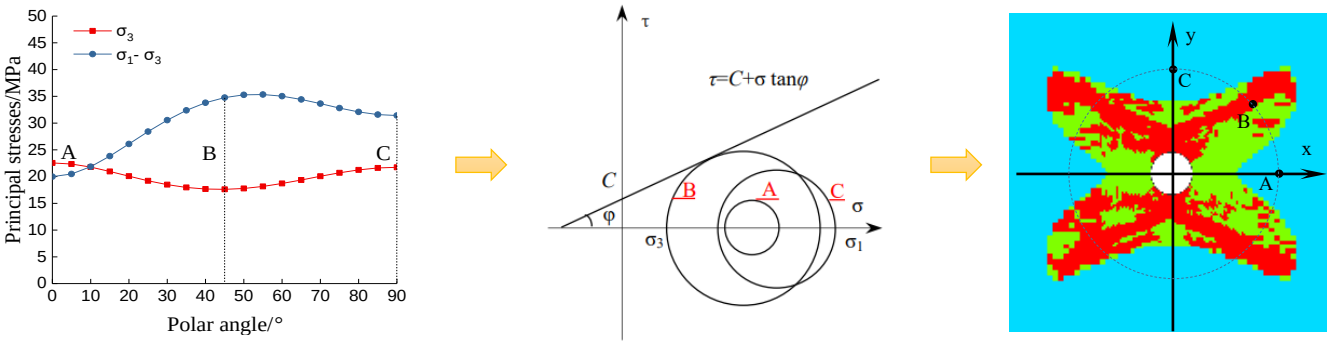

(a) Distribution of principal stress (b) Strength criterion (c) Circular plastic zone

Fig. 11 Formation mechanism of butterfly plastic zone

that is, circular plastic zone, as shown in Fig. 9(c).

4.3.2 Mechanical mechanism of elliptical plastic zone

The shape of plastic zone is elliptical when the model is under low partial confining stress ($1<\lambda<2$). In the circumferential direction, the minimum principal stress decreases and the principal stress difference increases with the polar angle, as shown in Fig. 10(a). In the figure, A represents the point on the circumferential abscissa axis, B represents the point on the middle axis in the first quadrant, and C represents the point on the circumferential ordinate axis. According to the distribution of principal stress, we can see that the radius of Mohr's circle at point C is the largest, followed by point B and the smallest at point a. At the same time, the minimum principal stress at point C is the smallest, followed by point B and the maximum at point A. The relative position relationship of Mohr's circle at points A, B and C is shown in the Fig. 10(b). The radius of Mohr's circle is the largest and the minimum principal stress is the smallest at point C, and the rock element is most likely to be destroyed here. The radius of Mohr's circle is the smallest and the minimum principal stress is the largest, and the rock element is least likely to be destroyed at point A. Therefore, under the condition of low partial confining stress, in any circumferential direction, the rock element at the abscissa axis is most likely to be destroyed, while it is the least likely to be destroyed at the ordinate axis, resulting in the formation of an elliptical plastic zone, as shown in Fig. 10(c).

4.3.3 Mechanical mechanism of butterfly plastic zone

The shape of plastic zone is butterfly when the model is under high partial confining stress state ($\lambda>2$). In the circumferential direction, the minimum principal stress decreases first and then increases, showing the characteristics of concave function; the principal stress difference increases first and then decreases, showing the characteristics of convex function, as shown in Fig. 11(a). The peak of the principal stress difference curve and the trough of the minimum principal stress curve are near the middle axis (θ=45°), as shown in point B in Fig. 11(a). The positions of the two axes are in the low position of the principal stress difference curve and the high position of the minimum principal stress curve, as shown in points A and C in Fig. 11(a). The relative position relationship of Mohr's circle at points A, B and C is shown in the Fig. 11(b). Therefore, under the condition of high partial confining stress, in any circumferential direction, the rock elements near the middle axis are easier to be destroyed, while the destructive force decreases gradually when it approaches the two axes, resulting in the formation of a butterfly plastic zone protruding in the quadrant and concave at the coordinate axis., as shown in Fig. 11(c).

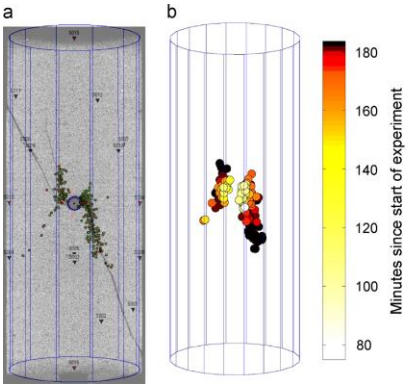

Fig. 12 Location of events (Aker *et al.* 2014)

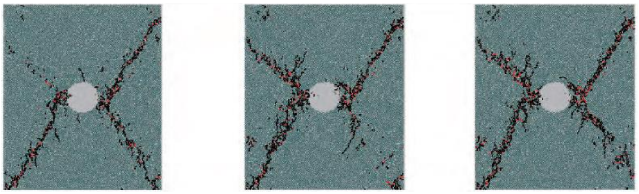

Fig. 13 Failure modes of specimens containing a single hole under biaxial compression (Li *et al.* 2017)

4.3.4 Comparison with the results previously published

There are many researches on the circular or elliptical plastic zone around the circular roadway in the existing literature, and the results have become part of academic orthodoxy. The research results of butterfly shaped plastic zone around roadway under high partial confining stress are relatively few. Most of the existing literatures are obtained from numerical simulation or laboratory tests.

Literature (Aker *et al.* 2014) studied the failure process of compressed sandstone sample with prefabricated holes by the acoustic emission test. Fig. 12 shows the statistical

chart of source location captured by acoustic emission during the test. It can be seen from the figure that the statistical figure of the source position obtained by the damage around the hole is similar to the butterfly distribution. Although the macro cracks around the holes in the test are different from those in the theoretical analysis, the macro cracks in the sample are similar to the two butterfly lobes in the butterfly shaped plastic zone, and the crack propagation position is also similar to that in the butterfly shaped plastic zone.

Literature (Li *et al.* 2017) used PFC2D software to study the crack growth process of the sample with holes under biaxial compression, and obtained the failure mode of the sample with holes under biaxial compression, as shown in Figure 13. The mode of macro cracks in the surrounding rock with holes in the non-uniform stress field is consistent with the theoretical results of the butterfly shaped plastic zone expansion law in this paper.

The uniaxial compression is that the confining pressure is 0 and the load is in the vertical direction, which constitutes the condition of partial confining stress. The butterfly failure of surrounding rock under partial confining stress is obtained by laboratory test conditions and different numerical simulation software. It can be seen that the theoretical results are reliable.

5. Discussions

We studied the distribution of principal stress field around a circular hole under partial confining stress from a microscopic view, and revealed the formation mechanism of plastic zones with different shapes. Next, we will discuss the influence of lateral stress coefficient and depth on the distribution of stress field from a macroscopic view, and further reveal the influence mechanism of lateral stress coefficient and depth on the shape of plastic zone.

5.1 The influence of the partial confining stress on principal stress field around circular hole

Taking the depth of 800 m as an example, we study the influence of the partial confining stress on principal stress field around circular hole. At the same time, the circumferential position of 3*a* is taken as a representative to explain the influence of lateral stress coefficient on principal stress difference and minimum principal stress, as shown in Fig. 14. With the increase of the lateral stress coefficient from 1, the principal stress difference generally increases, the curve gradually changes from straight line to convex curve, and the characteristics of convex function are gradually obvious (the peak increases and the low position at both ends decrease relatively), as shown in Fig. 14(a); the curve of minimum principal stress changes from straight line to concave curve, and the characteristics of convex function are gradually obvious (the trough decreases and the high position at both ends increase), as shown in Fig. 14(b).

The shape of the plastic zone is determined by the distribution characteristics of the principal stress field around the hole. The concavity and convexity of the minimum principal stress and the principal stress difference

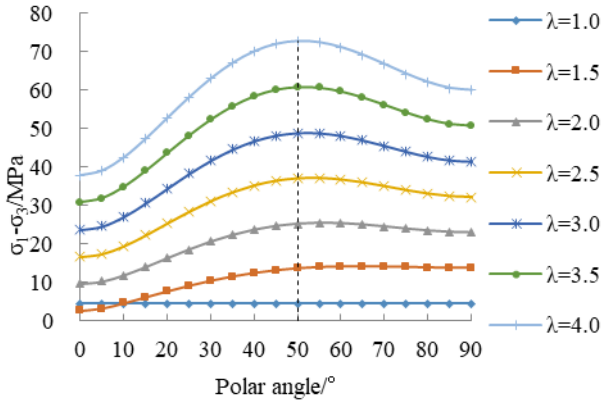

(a) Distribution of principal stress difference (r/a=3)

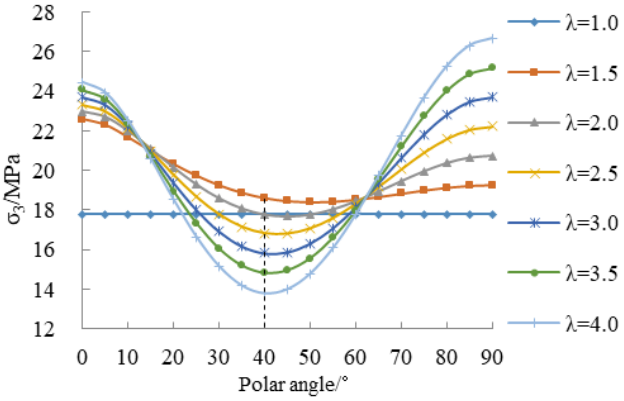

(b) Distribution of minimum principal stress (r/a=3)

Fig. 14 Distribution of principal stress with the lateral stress coefficient

results in the non-uniform distribution of the plastic zone around the circular hole, as shown in Fig. 11. In addition, the more concave the minimum principal stress curve is and the more convex the principal stress difference curve is, the more inhomogeneous the plastic zone distribution is, and the more obvious the butterfly feature is. Therefore, the lateral stress coefficient is the main factor causing the non-uniform failure of the roadway surrounding rock.

5.2 The influence of the depth on principal stress field around circular hole

Similarly, keeping the lateral stress coefficient at a fixed value of 2, we take the circumferential position of 3*a* as a representative to explain the influence of depth on principal stress difference and minimum principal stress, as shown in Fig. 15. With the increase of the depth, both principal stress difference and minimum principal stress increases exponentially as a whole, and it is equivalent to the curve moving upward in the coordinate system. The depth can only change the size of the principal stress around the hole, but not the concavity and convexity of the principal stress curve. This property can also be obtained by formula 4. In the formula stresses at any point can be expressed as a multiple function of depth. When the depth increases, the stress at each point will increase exponentially. The increase of depth will improve the overall level of the

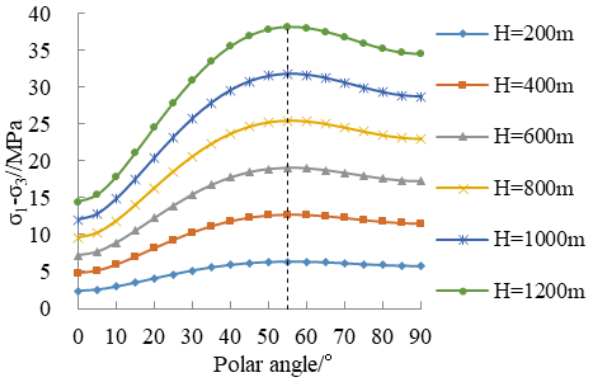

(a) Distribution of principal stress difference (r/a=3)

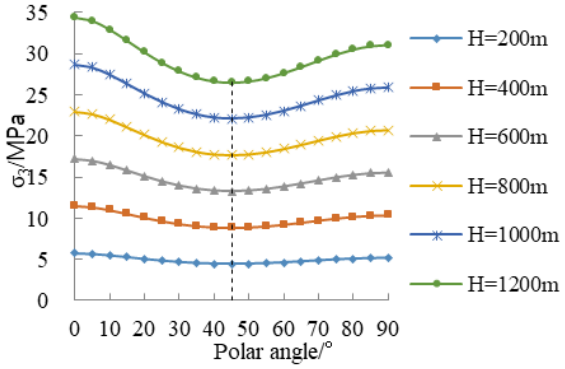

(b) Distribution of minimum principal stress (r/a=3)

Fig. 15 Distribution of principal stress with the depth

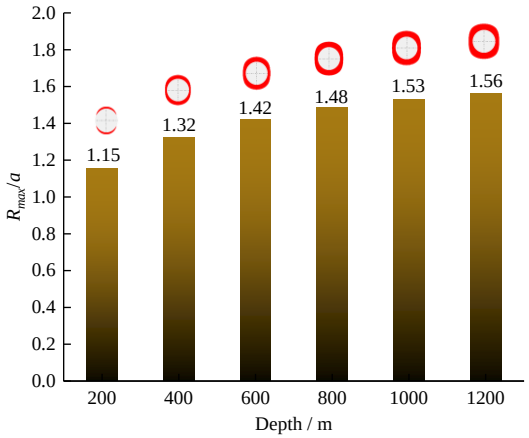

(a) Under low partial confining stress (λ=1.4)

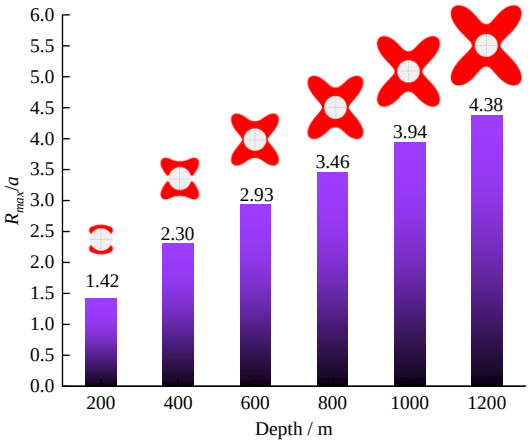

(b) Under high partial confining stress (λ=2.5)

Fig. 16 The influence of depth on the shape and size of plastic zone under partial confining stress (γ=25 KPa/m; C=3 MPa; φ=25°)

circumferential principal stress field and increase the failure range of surrounding rock. Therefore, the depth is the main factor causing the large-scale failure of the roadway surrounding rock.

5.3 The influence mechanism of the depth on the roadway plastic zone under partial confining stress

To reveal the influence mechanism of the depth on the roadway plastic zone under partial confining stress, we compare the shape and size of plastic zone under low and high partial confining stress, as shown in Fig. 16. R_{max} is the maximum radius from the center of the roadway to the boundary of the plastic zone, and the range of plastic zone is expressed by the ratio of maximum radius to roadway radius. The rock cohesion and internal friction angle in the model are 3 MPa and 25° respectively (Ma *et al.* 2015, Guo *et al.* 2016). We can see that the shape of plastic zone is elliptical under low partial confining stress, and that the size of the plastic zone increases gradually with the increase of depth. Similarly, the shape of plastic zone is butterfly under high partial confining stress, and that the size of the plastic zone increases gradually with the increase of depth. However, when the lateral stress coefficient is constant, the shape of plastic zone will not change with the depth increase. Therefore, the lateral stress coefficient is the main factor determining the shape of plastic zone, and the depth is the main factor determining the size of plastic zone.

The increase of depth will improve the overall level of the circumferential principal stress field and increase the failure range of surrounding rock. The increase of the lateral stress coefficient will enhance the concavity and convexity of the principal stress field around a circular hole and promote the non-uniform failure of surrounding rock. Under the condition of deep and high partial confining stress, the roadway surrounding rock will appear large-scale and non-uniform failure zone.

5.4 The guiding effect on engineering practice

This paper studied the shapes evolution and formation mechanism of the plastic zone surrounding circular roadway under partial confining stress in deep mining. Under the condition of deep and high partial confining stress, the roadway surrounding rock will appear large-scale and butterfly plastic zone, which will threaten the stability of the roadway surrounding rock. This study can guide the practice of roadway engineering from the following three aspects.

(1) Roadway layout

In the deep condition, the roadway should not be arranged in the high partial confining stress environment as far as possible. Before the excavation of roadway, based on the in-situ stress test results, the stress conditions in

different directions should be determined. The direction of roadway should be parallel to the direction of maximum principal stress rather than vertical. The roadway should be located in the stress environment where the plastic zone of surrounding rock is round or oval after excavation, and should not be arranged in the stress environment where the plastic zone of surrounding rock is butterfly.

(2) Roadway disaster prediction

By using theoretical method, the shape of plastic zone of roadway surrounding rock in a certain stress environment is judged, and the stability of roadway surrounding rock is mastered in advance. In the layout of the roadway, try to avoid the butterfly position. If the butterfly failure occurs in the surrounding rock of the roadway, timely measures should be taken to strengthen the support to avoid the occurrence of disasters.

(3) Roadway disaster control

This study provides a way for roadway disaster control under partial confining stress in deep mining. If the roadway is inevitably in the high partial confining stress environment, the stress environment can be destroyed by engineering means, such as unloading in the high stress direction, so as to improve the stress environment of the roadway.

6. Conclusions

In this study, we explored the shape evolution of the plastic zone surrounding circular roadway under partial confining stress in deep mining. We also studied the distribution of the principal stress field around the circular hole from the microscopic and macroscopic perspectives and revealed the formation mechanism of plastic zone with different shapes. Based on the work presented in this paper, the following conclusions are made:

(1) The formation mechanism of plastic zone with different shapes was revealed. Under hydrostatic stress (λ=1), the circumferential principal stress around the hole is the same everywhere, and the shape of plastic is circular; under low partial confining stress (1<λ<2), the rock element at the abscissa axis is most likely to be destroyed, while it is the least likely to be destroyed at the ordinate axis, resulting in the formation of an elliptical plastic zone; under high partial confining stress ($\lambda\geq$2), the rock elements near the middle axis are easier to be destroyed, while the destructive force decreases gradually when it approaches the two axes, resulting in the formation of a butterfly plastic zone.

(2) The concavity and convexity of the principal stress curve will be changed by the lateral stress coefficient, and the lateral stress coefficient is the main factor causing the butterfly failure of the roadway surrounding rock.

(3) The increase of depth will improve the overall level of the circumferential principal stress field and increase the failure range of surrounding rock. The depth is the main factor causing the large-scale failure of the roadway surrounding rock.

(4) Under the condition of deep and high partial confining stress, the roadway surrounding rock will appear large-scale and butterfly failure zone.

Acknowledgments

The authors wish to sincerely thank various organizations for their financial support. This work was partially supported by the National Natural Science Foundation of China (Grant no. 52004289) and the National Key Research and Development Program (Grant no. 2016YFC0600708).

Conflicts of interest

The authors declare no conflict of interest.

References

Aker, E., Kühn, D., Vavryčuk, V., Soldal, M. and Oye, V. (2014), "Experimental investigation of acoustic emissions and their moment tensors in rock during failure", *Int. J. Rock Mech. Min. Sci.*, **70**, 286-295. https://doi.org/10.1016/j.ijrmms.2014.05.003.

Atsushi, S., Duncan, M., Adam, K.S., Yuzo, O. and Murat, K. (2020), "Impact of the intermediate stress component in a plastic potential function on rock mass stability around a sequentially excavated large underground cavity", *Int. J. Rock Mech. Min. Sci.*, **127**, 104223. https://doi.org/10.1016/j.ijrmms.2020.104223.

Diederichs, M.S. (2018), "Early assessment of dynamic rupture hazard for rockburst risk management in deep tunnel projects", *J. S. Afr. I. Min. Metall.*, **118**(3), 193-204. https://doi.org/10.17159/2411-9717/2018/v118n3a1.

Detournay, E. and John, C.M.S. (1988), "Design charts for a deep circular tunnel under non-uniform loading", *Rock Mech. Rock Eng.*, **21**(2), 119-137. https://doi.org/10.1007/BF01043117.

Ding, L.J. and Liu, Y.H. (2018), "Study on deformation law of surrounding rock of super long and deep buried sandstone tunnel", *Geomech. Eng.*, **16**(1), 97-104. http://doi.org/10.12989/gae.2018.16.1.097.

Fan, L. and Liu, S.M. (2019), "Fluid-dependent shear slip behaviors of coal fractures and their implications on fracture frictional strength reduction and permeability evolutions", *Int. J. Coal Geol.*, **212**, 103235. https://doi.org/10.1016/j.coal.2019.103235.

Fan, W., Yu, M.H., Deng, LS., Peng, X.L. and Chen, L.W. (2013), "New strength formulae for rock surrounding a circular opening", *Can. Geotech. J.*, **50**(7), 735-743. https://doi.org/10.1139/cgj-2012-0001.

Feng, G.R., Wang, P.F., Chugh, Y.P. (2018), "Stability of gate roads next to an irregular yield pillar: A case study", *Rock Mech. Rock Eng.*, **52**(8), 2741-2760. https://doi.org/10.1007/s00603-018-1533-y.

Garavand, A., Stefanov, Y.P., Rebetsky, Y.L., Bakeev, R.A. and Myasnikov, A.V. (2020), "Numerical modeling of plastic deformation and failure around a wellbore in compaction and dilation modes", *Int. J. Numer. Anal. Met.*, **44**(6), 823-850. https://doi.org/10.1002/nag.3041.

Guo, X.F., Ma, N.J., Zhao, X.D., Zhao, Z.Q. and Li, Y.E. (2016), "The general shapes and criterion for surrounding rock mass plastic zone of round roadway", *J. China Coal Soc.*, **44**(8), 1871-1877. https://doi.org/10.13225/j.cnki.jccs.2016.0787.

Hill, R. (1950), *The Mathematical Theory of Plasticity*, Oxford University Press, Oxford, U.K.

Jiang, L., Sainoki, A., Mitri, H.S., Ma, N.J, Liu, H.T. and Hao, Z. (2016), "Influence of fracture-induced weakening on coal mine gateroad stability", *Int. J. Rock Mech. Min. Sci.*, **88**, 307-317.

https://doi.org/ 10.1016/j.ijrmms.2016.04.017.
Kang, H., Zhang, X., Si, L., Wu, Y. and Gao, F. (2010), "In-situ stress measurements and stress distribution characteristics in underground coal mines in China", *Eng. Geol.*, **116**, 333-345. https://doi.org/345. 10.1016/j.enggeo.2010.09.015.
Kastner, H. (1971), *Statik des Tunel und Stollenbauess*, Springer, Berlin Heidelberg, Germany.
Konicek, P., Soucek, K., Stas, L. and Singh, R. (2013), "Long-hole destress blasting for rockburst control during deep underground coal mining", *Int. J. Rock Mech. Min. Sci.*, **61**, 141-153. https://doi.org/10.1016/j.ijrmms.2013.02.001.
Lamich, D., Marschalko, M., Yilmaz, I., Bednářová, P., Niemiec, D., Kubečka, K. and Mikulenka, V. (2016), "Subsidence measurements in roads and implementation in land use plan optimisation in areas affected by deep coal mining", *Environ. Earth Sci.*, **75**(1), 1-11. https://doi.org/10.1007/s12665-015-4933-2.
Leitman, M.J. and Villaggio, P. (2009), "Plastic zone around circular holes", *J. Eng. Mech.*, **135**(12), 1467-1471. https://doi.org/10.1061/(ASCE)EM.1943-7889.0000062.
Li, C.J., Li, X.B., Li, D.Y. (2017), "Particle flow analysis of fracture characteristics of marble with a single hole", *Chin. J. Eng.*, **39**(12), 1791-1801. https://doi.org/10.13374/j.issn2095-9389.2017.12.003.
Li, C., Zhang, W.L., Wu. Z, Sun, Y.H., Zhu, C. and Zhang, X.H. (2020), "A case study on asymmetric deformation mechanism of the reserved roadway under mining influences and its control techniques", *Geomech. Eng.*, **22**(5), 449-460. http://dx.doi.org/10.12989/gae.2020.22.5.449
Li, P., Cai, M.F., Guo, Q.F. and Miao, S.J. (2019), "In situ stress state of the northwest region of the jiaodong peninsula, China from overcoring stress measurements in three gold mines", *Rock Mech. Rock Eng.*, **52**(11), 4497-4507. https://doi.org/10.1007/s00603-019-01827-3.
Liu, J.H., Jiang, F.X., Wang, N.G., Li, Z.S. and Zhang, Z.G. (2012), "Research on reasonable width of segment pillar of fully mechanized caving face in extra-thick coal seam of deep shaft", *Chin. J. Rock Mech. Eng.*, **31**(5), 921-927. https://doi.org/10.1007/s11783-011-0280-z.
Ma, N.J., Li, J. and Zhao, Z.Q. (2015), "Distribution of the deviatoric stress field and plastic zone in circular roadway surrounding rock", *J. China U. Min. Technol.*, **44**, 206-213. https://doi.org/10.13247/j.cnki.jcumt.000309.
Maihemuti, B., Wang, E.Z., Hudan, T. and Xu, Q.J. (2016), "Numerical simulation analysis of reservoir bank fractured rock-slope deformation and failure processes", *Int. J. Geomech.*, **16**(2), 04015058. https://doi.org/10.1061/(ASCE)GM.1943-5622.0000533.
Palumbo, D., De Finis, R., Ancona, F. and Galietti, U. (2017), "Damage monitoring in fracture mechanics by evaluation of the heat dissipated in the cyclic plastic zone ahead of the crack tip with thermal measurements", *Eng. Fract. Mech.*, **181**, 65-76. https://doi.org/10.1016/j.engfracmech.2017.06.017.
Paul, S.K. (2016), "Numerical models of plastic zones and associated deformations for elliptical inclusions in remote elastic loading–unloading with different R-ratios" *Eng. Fract. Mech.*, **152**, 72-80. https://doi.org/10.1016/j.engfracmech.2015.12.008.
Poulos, H.G. and Davis, E.H., (1974), *Elastic Solutions for Soil and Rock Mechanics*, Wiley, New York, U.S.A.
Tian, M.L., Han, L.J., Meng, Q.B., Ma, C., Zong, Y.J. and Mao, P.Q. (2020), "Physical model experiment of surrounding rock failure mechanism for the roadway under deviatoric stress form mining disturbance", *KSCE J. Civ. Eng.*, **24**(4), 1103-1115. https://doi.org/10.1007/s12205-020-1540-x.
Rezaei, M., Hossaini, M.F. and Majdi, A. (2015), "Determination of longwall mining-induced stress using the strain energy Method", *Rock. Mech. Rock. Eng.*, **48**(6), 2421-2433. https://doi.org/10.1007/s00603-014-0704-8
Vazaios, I., Vlachopoulos, N. and Diederichs, M.S. (2019), "Assessing fracturing mechanisms and evolution of excavation damaged zone of tunnels in interlocked rock masses at high stresses using a finite-discrete element approach", *J. Rock Mech. Geotech.*, **11**(4), 701-722. https://doi.org/ 10.1016/j.jrmge.2019.02.004.
Vidigal-Souza, P.A., Vilas-Boas, D.B., Brandão, A.G. and Holz, M., (2020), "Seismic stratigraphy of camamu basin, Northeastern Brazil", *Pure Appl. Geophys.*, **177**(11), 5207-5224. https://doi.org/ 10.1007/s00024-020-02580-3.
Vitali, O.P.M., Celestino, T.B. and Bobet, A. (2020), "Analytical solution for a deep circular tunnel in anisotropic ground and anisotropic geostatic stresses", *Rock Mech. Rock Eng.*, **53**(6), 3859-3884. https://doi.org/10.1007/s00603-020-02157-5.
Wang, S.F., Huang, L.Q. and Li, X.B. (2020), "Analysis of rockburst triggered by hard rock fragmentation using a conical pick under high uniaxial stress", *Tunn. Undergr. Sp. Tech.*, **96**(2), 103195. https://doi.org/10.1016/j.tust.2019.103195.
Yang, D.W., Ma, Z.G., Qi, F.Z., Gong, P., Liu, D.P., Zhao, G.Z. and Zhang. R.C. (2017a), "Optimization study on roof break direction of gob-side entry retaining by roof break and filling in thick-layer soft rock layer", *Geomech. Eng.*, **13**(2), 195-215. http://doi.org/10.12989/gae.2017.13.2.195.
Yang, S.Q., Chen, M., Jing, H.W., Chen, K.F. and Meng, B. (2017b), "A case study on large deformation failure mechanism of deep soft rock roadway in Xin'an coal mine, china", *Eng. Geol.*, **217**, 89-101. https://doi.org/10.1016/j.enggeo.2016.12.012.
Zhu. C., Chang, Y., Cui, X.B., Ren, F.Q. and Zhang, X.H. (2019), "Study on the size effect of fracture intersections based on the fractal theory", *Geotech. Geol. Eng.*, **37**(4), 2999-3006. https://doi.org/10.1007/s10706-019-00818-z.

CC